A&A 521, A25 (2010)
DOI: 10.1051/0004-6361/201015210

Astronomy & Astrophysics

Potential vorticity dynamics in the framework of disk shallow-water theory

I. The Rossby wave instability

O. M. Umurhan[1,2]

[1] School of Mathematical Sciences, Queen Mary University of London, London E1 4NS, UK
e-mail: umurhan@maths.qmul.ac.uk
[2] Astronomy Department, City College of San Francisco, San Francisco, CA 94112, USA

Received 14 June 2010 / Accepted 13 July 2010

ABSTRACT

Context. The Rossby wave instability in astrophysical disks is a potentially important mechanism for driving angular momentum transport in disks.
Aims. We attempt to more clearly understand this instability in an approximate three-dimensional disk model environment which we assume to be a single homentropic annular layer we analyze using disk shallow-water theory.
Methods. We consider the normal mode stability analysis of two kinds of radial profiles of the mean potential vorticity: the first type is a single step and the second kind is a symmetrical step of finite width describing either a localized depression or peak of the mean potential vorticity.
Results. For single potential vorticity steps we find there is no instability. There is no instability when the symmetric step is a localized peak. However, the Rossby wave instability occurs when the symmetrical step profile is a depression, which, in turn, corresponds to localized peaks in the mean enthalpy profile. This is in qualitative agreement with previous two-dimensional investigations of the instability. For all potential vorticity depressions, instability occurs for regions narrower than some maximum radial length scale. We interpret the instability as resulting from the interaction of at least two Rossby edgewaves.
Conclusions. We identify the Rossby wave instability in the restricted three-dimensional framework of disk shallow water theory. Additional examinations of generalized barotropic flows are needed. Viewing disk vortical instabilities from the conceptual perspective of interacting edgewaves can be useful.

Key words. hydrodynamics – accretion, accretion disks – instabilities

1. Introduction

The Rossby wave instability (hereafter RWI) is a promising candidate mechanism to account for the observed anomalous transport of cold astrophysical disks[1]. The process involves the instability of waves in an environment in which there are radial variations in a potential vorticity quantity (PV hereafter). This effect is the disk analog of the Rayleigh instability of stably stratified barotropic shear flows that are familiar in meteorology and geophysical fluid dynamics. The original works wherein the RWI was proposed for disks (Lovelace et al. 1999; Li et al. 2000; Li et al. 2001) demonstrated the existence and evolution of the instability in vertically integrated disk models. The earliest known (to this author) identification of the relevance of PV dynamics to astrophysical settings is found in Lovelace & Hohlfeld (1978) containing a study of the stability of cold self-gravitating galactic disks subjected to radially localized perturbations. For the galactic disk study as well as the RWI, instability requires the existence of a minimum or maximum in the associated radial PV-profile of the disk[2].

Because of the potential importance of this mechanism for disks, it is worthwhile to consider and understand this instability in disk settings, which are three dimensional, at least in part. The goal of this study is to expose the machinery of this process as clearly as possible in the context of a three-dimensional theory.

Disk shallow water theory (Umurhan 2008, and hereafter DSW-theory) is a model reduction of the disk equations that is three-dimensional but asymptotic in the sense that azimuthal scales are much larger than the corresponding vertical and radial scales. It is essentially a model environment representing vortex dynamics occurring on thin annular sections of disks over timescales which are much longer than the local disk rotation time. The original motivation for this approximation was to develop a three-dimensional framework to describe the dynamics of elongated vortices known to emerge in two-dimensional studies such as that reported in Godon & Livio (1999). The benefit of using the DSW-theory is that it allows a transparent analysis of vortex dynamics free of other physical processes that are likely not to play a significant role – in particular, free of both acoustic and gravity mode oscillations. As such, by means of this framework one may develop a mechanical understanding of disk-related vortex dynamics.

In Umurhan (2008), DSW-theory was applied to understand the emergence of one form of the strato-rotational instability, which is an instability of a stably stratified Rayleigh stable shear profile in a channel (Yavneh 2001; Dubrulle et al. 2005). The no-normal flow boundary conditions at the walls of the domain

[1] I.e., non-magnetized disks.
[2] Note that in Lovelace & Hohlfeld (1978) the associated quantity $f(r)$ corresponds roughly to the inverse of the PV.

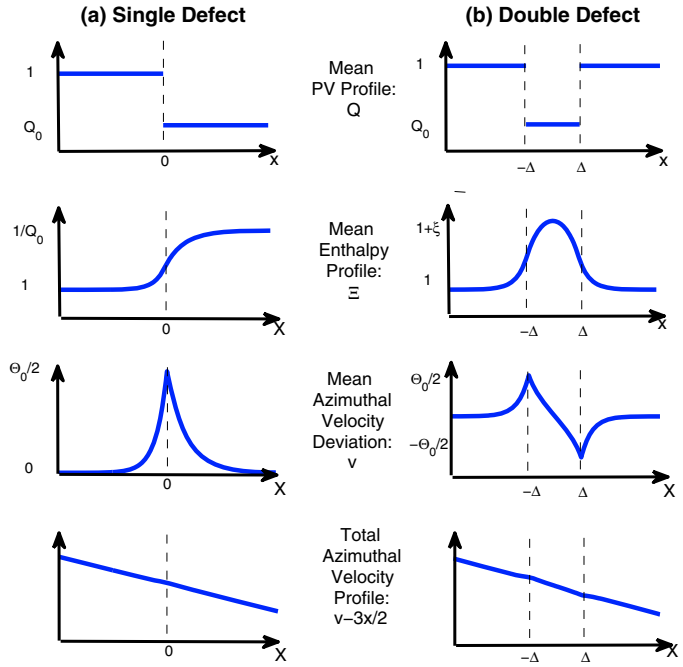

Fig. 1. Sketches of profile plots considered in this work. **a)** Single defect/jump located at $x = 0$. **b)** Double defect (symmetric step) with jumps located at $x = \pm\Delta$. Double defect depicted is a depression whose mean (midplane) enthalpy profile corresponds to a peak.

bring into existence edgewaves (e.g., Goldreich et al. 1986) that propagate along the walls in opposite directions with respect to one another. However, because the edgewaves may also interact with one another across the domain, if the separation of the walls fall within a specific allowed range, then the phase speeds of the edgewaves can "resonate" with each other and become unstable (Umurhan 2006; Umurhan 2008).

This edgewave dynamical picture has been used to understand the development of many forms of potential vorticity driven geophysical fluid instabilities including, among others, the original problem considered by Rayleigh (Hoskins et al. 1985; Baines & Mitsudera 1994; Heifetz et al. 1999) as well as astrophysical processes such as the Papaloizou-Pringle instability (Papaloizou & Pringle 1984; Goldreich et al. 1985). In the geophysical fluid dynamics context, this is frequently referred to as the instability of counter-propagating Rossby waves (e.g., Heifetz et al. 1999). The use of edgewaves as an interpretive tool has precedence in the analysis of plasma instabilities. For example, the diocotron effect, which is an instability associated with finite thickness charge sheets subjected to $E \times B$ drift, is rationalized to arise from the interaction of edgewaves counter-propagating along the surfaces of the charge sheet (Knauer 1966).

DSW-theory is an appropriate platform to examine the RWI. Indeed, an examination of the vortex structures emerging from nonlinear calculations of the instability (see Fig. 1 of Li et al. 2000, hereafter LFLC-2000) shows that the coherent vortex structure is severely elongated in the azimuthal direction while being radially tightly confined. This structural quality is similar to the vortices reported in Godon & Livio (1999). The advantage of DSW-theory is that it can capture some essence of three-dimensionality, while its disadvantage is that, because of its construction, small azimuthal scales cannot be represented. By contrast, the vertically integrated model environment used in the original RWI studies are able to capture small azimuthal scales while coming at the expense of representing three-dimensionality.

In this study, the RWI is examined in the framework of DSW-theory. The stability of two analytically tractable mean PV-profiles is studied: (i) a single defect, or "single-step"; and (ii) a double defect, or "symmetric-step" (see Fig. 1). As in the case of the stratorotational instability, the RWI is shown to result from the interaction of Rossby edgewaves that propagate along the locations of the steps of the mean PV-profile. However, the instability manifests itself only in the symmetric step case. In Sect. 2, the equations of motion and their perturbations are presented. In Sect. 3, the equations are analyzed for two kinds of mean potential vorticity profiles including the one just described. Analytic solutions are determined throughout by considering the quasi-linear problem posed by considering the special case $\gamma = 3$, where γ is the ratio of specific heats. Section 4 concludes with comments and a discussion about recent three-dimensional RWI calculations (Meheut et al. 2010).

2. Equations and potential vorticity conservation

The asymptotic equations upon which DSW-theory is based, describing the evolution of annular disk sections, was developed in Umurhan (2008). In that study, the equations of motion for an annular section in which the vertical/radial extent $\mathcal{L}$ is much smaller that the azimuthal scale R was developed as an asymptotic series expansion in powers of $\epsilon \equiv \mathcal{L}/R$. The timescales of the dynamics ($\mathcal{T}$) is comparatively long with respect to the local rotation time $(1/\Omega_0)$ of the annular disk centered on R_0 i.e., $\mathcal{T} \sim 1/(\epsilon\Omega_0)$. To ensure a non-trivial asymptotic balance, the radial and vertical velocities viewed in the reference frame of the annulus rotating with Ω_0 must scale as ϵc_s where c_s is the sound speed of the gas, while the corresponding deviations of the azimuthal velocities must scale as c_s. This disparity in aspect and velocity ratios is an asymptotic description of azimuthally elongated slowly overturning vortices. Furthermore, the reduced equations of motion in the annular disk section possess quasi-geostrophic characteristics familiar in meteorological studies.

Single constant entropy layers are considered when the equation of state is polytropic, i.e., it is assumed that $P = K\rho^\gamma$ everywhere at all times. This corresponds to a situation in which the specific entropy inside, defined by $S = C_v \ln(P/\rho^\gamma) = C_v \ln K$, is everywhere a constant. This homentropic layer is considered in the following. If there are radial variations of the mean height of the disk (h), then the *vertically integrated* entropy of the disk also exhibits radial variations even though the specific entropy is constant. This point is made to keep in mind how the equations analyzed here compares to the vertically integrated two-dimensional equations studied in Li et al. (2000).

After non-dimensionalizing all the quantities according to the above, the leading order equations describing the evolution of varicose disturbances of a single constant specific entropy layer are

$$v = \tfrac{1}{2}\partial_x \Xi, \tag{1}$$

$$\frac{Dv}{Dt} + (2-q)u = -\partial_y \Xi, \tag{2}$$

$$\frac{D\Xi}{Dt} = 2\Xi\Omega_z, \tag{3}$$

$$\partial_x u + \partial_y v + \frac{\gamma+1}{\gamma-1}\Omega_z = 0, \tag{4}$$

where x, y represent the non-dimensional radial and azimuthal coordinates and t is the non-dimensionalized time (Umurhan 2008). In this construction, all quantities appearing are functions of these two coordinates and time. The radial velocity is u. The total time derivative is

$$\frac{\mathrm{D}}{\mathrm{D}t} \rightarrow \partial_t + (v - qx)\partial_y + u\partial_x.$$

The background shear $= -qx\vec{j}$, is linear in the radial coordinate. For a Keplerian disk, $q = 3/2$. Thus, the azimuthal velocity v appearing here is understood to be a deviation from this basic background state as viewed in the local rotating frame. The quantity Ξ may be understood to be the enthalpy of the disk midplane and is given by

$$\Xi = \tfrac{1}{2}h^2, \tag{5}$$

where $h = h(x, y, t)$ corresponds to the height of the disk measured from the disk midplane. The height h is the position at which the enthalpy goes to zero in the constant (specific) entropy environment. Although Ξ is technically the *midplane enthalpy*, it is referred to hereafter as simply the *enthalpy* with full understanding that it is really its value at the midplane.

Equation (1) is the radial momentum balance equation but in this asymptotic limit it says that all perturbations are radially geostrophic. Equation (2) is the azimuthal momentum balance and, unlike the radial version, no geostrophic balance is implied. Equations (3) and (4) represent, respectively, the motion of the surface h and an equation of state for the gas (see below). In the derivation contained in Umurhan (2008), these two equations result from (i) exploiting the hydrostasy of perturbations at all times and (ii) an analysis of the energy equation, which makes use of the linear independence of powers of z.

The disk vertical velocity, though not explicitly appearing, is odd symmetric with respect to the disk midplane because of the assumed varicose symmetry of the disk response. In the development of the DSW-theory its functional form is shown to be $w = z\Omega_z(x, y, t)$. In the reduction leading to these equations only $\partial_z w$ appears as well as the explicit evaluation of the velocity of the layer at the height $z = h$. Additional details are found in Umurhan (2008).

The combination of these equations of motion leads to the conservation of potential vorticity Q given by

$$\frac{\mathrm{D}Q}{\mathrm{D}t} = 0, \qquad Q \equiv \frac{2(2-q) + \partial_x^2\Xi}{\Xi^{\frac{1}{2}\frac{\gamma+1}{\gamma-1}}}\,. \tag{6}$$

The next section considers the fate of normal modes for potential vorticity (or "PV" for short) profiles in which there is either a single or a double defect in the steady PV profile $Q = \bar{Q}(x)$.

3. Analytical study

The analysis in this work considers the fate of disturbances where $\gamma = 3$. This is chosen because the resulting equations, both steady and normal mode disturances, may be analyzed without intensive use of numerical methods. General more realistic values of γ require numerical evaluation of both the steady and time-depenedent state and this will be reserved for a future study. For $\gamma = 3$, the PV expression takes on the quasi-linear form

$$Q = \frac{2(2-q) + \partial_x^2\Xi}{\Xi}\,. \tag{7}$$

The following sections consider the two analytically tractable defect profiles and their normal mode responses.

3.1. Single defect

In this study, the term *defect* is used to indicate places where steps occur in the mean PV-profile. The following simple single defect,

$$\bar{Q} = \begin{cases} 1, & x < 0, \\ Q_0 & x > 0, \end{cases} \tag{8}$$

is studied. The value of Q_0 is constrained to be greater than zero. Solutions are sought that are bounded as $x \rightarrow \pm\infty$. This means solving for the mean enthalpy $\bar{\Xi}$

$$\partial_x^2\bar{\Xi} - \bar{Q}\bar{\Xi} = -1, \tag{9}$$

on either side of $x = 0$ (and where $q = 3/2$ has been explicitly used). The particular boundary conditions for the profiles at infinity are (i) $\bar{\Xi} \rightarrow 1$ as $x \rightarrow -\infty$ and (ii) $\bar{\Xi} \rightarrow 1/Q_0$ as $x \rightarrow \infty$. At the interface $x = 0$, it is also required that $\bar{\Xi}$ and its radial gradient $\partial_x\bar{\Xi}$ are matched, the latter being identical to requiring the matching of the azimuthal velocities $\bar{v}$ from both sides. The solution for the mean enthalpy is therefore

$$\bar{\Xi} = \begin{cases} 1 + \Theta_0 \mathrm{e}^{x}, & x < 0, \\ 1/Q_0 - \Theta_0/\sqrt{Q_0}\mathrm{e}^{-\sqrt{Q_0}x} & x > 0, \end{cases} \tag{10}$$

where

$$\Theta_0 = \left(\frac{1-Q_0}{Q_0}\right)\frac{\sqrt{Q_0}}{1+\sqrt{Q_0}}\,. \tag{11}$$

This result may be read to mean that the mean height $\bar{h}$ decreases when $Q_0 > 1$ and increases when $0 < Q_0 < 1$. It follows from Eq. (1) that

$$\bar{v} = \tfrac{1}{2}\begin{cases} \Theta_0\mathrm{e}^{x}, & x < 0, \\ \Theta_0\mathrm{e}^{-\sqrt{Q_0}x}, & x > 0, \end{cases} \tag{12}$$

which means that the deviation velocity at $x = 0$ is given by $\bar{v}_0 = \Theta_0/2$. As $x \rightarrow \pm\infty$, the mean velocity deviation goes to zero. The mean states developed here are qualitatively sketched in Fig. 1.

Infinitesimal perturbations of this steady state are introduced by writing for each dependent quantity $F \rightarrow \bar{F} + F'$, where $F'(x, y, t)$ is small compared to the basic state $\bar{F}$. This means that the potential vorticity equation is

$$\Big[\partial_t + (\bar{v} - 3x/2)\partial_y\Big]Q' + u'\frac{\mathrm{d}\bar{Q}}{\mathrm{d}x} = 0, \tag{13}$$

where Q' is given as

$$Q' = \frac{\partial_x^2\Xi' - \bar{Q}\Xi'}{\bar{\Xi}}.$$

Because $\mathrm{d}\bar{Q}/\mathrm{d}x$ entails a delta-function at $x = 0$, special well-known treatments must be utilized to solve these equations (for example, see Drazin & Reid 1982). For this type of problem, the procedure is detailed, for example, in Umurhan (2008), and may be summarized as follows: (i) solve $Q' = 0$ on either side of the defect; (ii) match Ξ' coming in from both sides; and (iii) make sure that the normal velocities u' are matched across the boundary. The last of these may be straightforwardly enforced by inspecting the linearized version of Eq. (2),

$$\Big(\partial_t + (\bar{v} - qx)\partial_y\Big)\partial_x\Xi' + \Big(4 - 2q + \partial_x^2\bar{\Xi}\Big)u' = -2\partial_y\Xi', \tag{14}$$

and requiring that the two solutions coming in from either side of $x = 0$ satisfy the requirement that the normal velocities u' are the same there.

Normal mode solutions of the form $\Xi' = \hat{\Xi}(x) \exp i\alpha(y - ct)$ are assumed. Solutions with $c > 0$ correspond to waves that propagate in the forward y direction and, correspondingly, in the negative y direction for $c < 0$. It follows that the solution for Ξ', away from the two boundaries, satisfying the condition that their amplitudes are equal at $x = 0$ and, $\hat{\Xi} \to 0$ as $x \to \pm\infty$, is

$$\hat{\Xi} = A_0 \begin{cases} e^{x}, & x < 0, \\ e^{-\sqrt{Q_0}x}, & x > 0, \end{cases} \tag{15}$$

where A_0 is an arbitrary constant. The requirement that the normal perturbation velocities, u', match at the defect location means ensuring that

$$\left[\frac{(\bar{v}_0 - c - 3x/2)\partial_x \hat{\Xi} + 2\hat{\Xi}}{1 + \partial_x^2 \hat{\Xi}} \right]_{x \to 0^-}^{x \to 0^+} = 0. \tag{16}$$

Satisfaction of this condition leads to an eigenvalue condition on the wavespeed c which, after some algebra, reduces to the simple form

$$c - \bar{v}_0 = -2\Theta_0 = -4\bar{v}_0. \tag{17}$$

For $\bar{v}_0$ given above, it follows that that $c = -3\bar{v}_0$. The wave here is a Rossby edgewave phenomenon (e.g. Baines Mitsudera 1994) and the eigenvalue determined here describes the speed with which the edgewave propagates. If the defect were placed at some position other than $x = 0$, then the observed speed of the edgewave would be Doppler-shifted according to the Keplerian velocity at the position of the defect. Thus, if the defect were instead at $x = x_0$, the wavespeed would then be given by $c = -3x_0/2 - 3\bar{v}_0$.

3.2. Double defect: the symmetric step

This subsection is an analysis of a symmetrical defect pair. The previous section demonstrates how a single defect produces a single Rossby edgewave along the defect. For two defects, therefore, two Rossby edgewaves are expected and it is under these circumstances that instability may emerge according to the principles of interacting waves (Hayashi & Young 1985; Baines & Mitsudera 1994; Heifetz et al. 1999).

The mean PV-profile appropriate for a double symmetric defect is

$$\bar{Q} = \begin{cases} 1, & x < -\Delta, \\ Q_0, & -\Delta < x < \Delta, \\ 1, & x > \Delta, \end{cases} \tag{18}$$

where $\Delta > 0$. The edges of the defect are located at $x = \pm\Delta$ and separated by a distance 2Δ, where Δ is the region's half-width. Following the same procedures as outlined in the previous section and requiring that $\bar{\Xi} \to 1$ as $x \to \pm\infty$, the mean enthalpy is found to be

$$\bar{\Xi} = \begin{cases} \Theta_0 e^{x+\Delta} + 1, & x < -\Delta, \\ \frac{1}{Q_0} - \frac{\Theta_0}{\sqrt{Q_0}} \frac{\cosh \sqrt{Q_0}x}{\sinh \sqrt{Q_0}\Delta}, & -\Delta < x < \Delta, \\ \Theta_0 e^{-x+\Delta} + 1, & x > \Delta. \end{cases} \tag{19}$$

The value of Θ_0 in this case is

$$\Theta_0 = \frac{1 - Q_0}{Q_0} \cdot \frac{\sqrt{Q_0} \tanh \sqrt{Q_0}\Delta}{1 + \sqrt{Q_0} \tanh \sqrt{Q_0}\Delta}. \tag{20}$$

It means that for $0 < Q_0 < 1$, the enthalpy deviation is a *peak* or *bump*, while for $Q_0 > 1$ the enthalpy structure is a *depression*. The corresponding mean velocity deviations are

$$\bar{v} = \frac{1}{2} \begin{cases} \Theta_0 e^{x+\Delta}, & x < -\Delta, \\ -\Theta_0 \frac{\sinh \sqrt{Q_0}x}{\sinh \sqrt{Q_0}\Delta}, & -\Delta < x < \Delta, \\ -\Theta_0 e^{-x+\Delta}, & x > \Delta. \end{cases} \tag{21}$$

Defining $\bar{v}(\pm\Delta) \equiv \bar{v}(x = \pm\Delta)$, it follows that at the defects $\bar{v}(\pm\Delta) = \mp\Theta_0/2$. It is useful to define ξ, i.e., the ratio of the height of the peak mean enthalpy to its value as $x \to \pm\infty$,

$$\xi \equiv \frac{\max(\bar{\Xi})}{\bar{\Xi}(\pm\infty)} = \frac{1}{Q_0} - \frac{\Theta_0}{\sqrt{Q_0}} \frac{1}{\sinh \sqrt{Q_0}\Delta}. \tag{22}$$

A qualitative sketch of the mean states are depicted in Fig. 1.

Because there are two defects, individual edgewaves propagate along each of them, which interact with each other as well. A normal-mode analysis, as executed in the previous section, is performed. The details are presented in the Appendix. The resulting wavespeed c satisfies the relationship

$$c^2 = \mathcal{E}, \tag{23}$$

where

$$\mathcal{E}(Q_0, \Delta) = \frac{3(Q_0 - 1)}{4Q_0} \left\{ 1 + \frac{4\beta}{\sqrt{Q_0}} - \frac{3\beta^2}{1 - Q_0} - \frac{1}{(\cosh\beta + \sqrt{Q_0}\sinh\beta)^2} + \frac{4\left(\beta + \sqrt{Q_0}\right)\sinh\beta\left[(Q_0 - 2)\cosh\beta - \sqrt{Q_0}\sinh\beta\right]}{2Q_0\cosh 2\beta + \sqrt{Q_0}(1 + Q_0)\sinh 2\beta} \right\},$$

and $\beta \equiv \sqrt{Q_0}\Delta$ is defined for convenience. The results of this are plotted in Fig. 3. The first clear result is that instability ($\mathcal{E} = 0$) may only occur for enthalpy bumps, which is to say that instability occurs for PV-depressions, $0 < Q_0 < 1$. The boundary between stable and unstable parameter regimes as a function of Q_0 is given by $\Delta_{cr}(Q_0)$. Thus, for PV-depressions, instability occurs for $0 < \Delta < \Delta_{cr}$. For very small but non-zero values of Q_0, the results show that $\Delta_{cr} \sim Q_0^{-1/2}$. Defining instead Q_{cr} as the marginally stable value of the PV-depression then its asymptotic form has the functional dependence $\sim\Delta^{-2}$ for $\Delta \gg 1$. Figure 4 shows plots of the wavespeeds as a function of Δ for representative values of a PV depression and peak.

4. Comments and discussion

It has been shown that the RWI is recovered in the framework of DSW-theory. The RWI emerges when the idealized symmetric-step mean (radial) potential-vorticity profile is a depression (or equivalently, when the mean radial enthalpy profile is a peak). However, single stepped mean PV profiles do not support the instability. The RWI is interpreted as being caused by the interaction of two Rossby-edgewaves propagating azimuthally along each defect of the symmetric step PV-profile. These types of dynamical processes are a generic feature of many vortical dynamics in geophysical flows. Below is a collection of comments

about these results including comparisons between the results of this work and the original RWI studies:

1. A weakness of the analysis performed here is that an unrealistic value of the ratio of specific heats was used: a value of $\gamma = 3$ places the fluid in a thermodynamic regime somewhere between a normal gas and an incompressible fluid (the latter being $\gamma \to \infty$, Salby 1989). The main reason for this choice was to develop the analysis analytically as most other values of γ require numerical methods to study both the steady states and the perturbation evolution. Among other things, developing analytical solutions are important for benchmarking future analyses for more reasonable values of γ. But most of all, the analytical solutions offer the most transparency in interpreting the results. Preliminary calculations for realistic values of γ show that the main mechanical interpretations and qualitative solutions, as well as conditions for onset, are not considerably altered. This is the subject of a study in preparation.

2. The limiting form of the DSW-theory used to study the RWI considers the response of a single homentropic disk layer. In this picture, the mean vertical height of the disk is a function of the radial coordinate, i.e., $\bar{h} = \bar{h}(x)$. Instability only occurs when the enthalpy of the disk layer (which is $\propto \bar{h}^2$) has a peaked structure. In LFLC-2000, the RWI is demonstrated in a vertically integrated model of a disk. Similar in quality to the results here, instability occurs when there is a peak in the mean radial pressure profile (or, relatedly, the surface density profile). In contrast, however, instability occurs for constant specific entropy profiles. This might imply that these results conflict with one another.

Because the disk model considered in LFLC-2000 is vertically integrated, all of the fluid quantities considered there are also understood to be vertically integrated, including the entropy. In the DSW-theory framework studied here, despite the specific entropy being constant throughout the layer, its vertical integration is not constant if the mean height of the disk is not uniform. That is to say if one defines

$$\mathcal{S} = \int_{\bar{h}}^{-\bar{h}} S \, \mathrm{d}z = 2\bar{h} C_v \ln K,$$

as the vertically integrated specific entropy of the disk, then it is self-evident that $\mathcal{S}$ is not uniform if $\bar{h}$ varies with radius x. As such, the results of this study should be compared to the non-homentropic incarnations of the RWI discussed in the original studies, for example, as in Li et al. (2001).

3. With respect to the last point, the version of the RWI uncovered in the analysis of the symmetric step is qualitatively similar to the homentropic Gaussian bump profile ("HGB") considered in LFLC-2000, where HGB describes the quality of the radial dependence of the mean pressure. However, as stated above, the symmetric step profile studied in this work is effectively non-homentropic when viewed in terms of the vertically integrated disk model considered in Li et al. (2000). The symmetric step profile might, therefore, most closely correspond to a *non-homentropic Gaussian bump profile* ("NGB") in the framework of the vertically integrated model of LFLC-2000. A NGB profile was examined in the nonlinear regime in Li et al. (2001), and, in a qualitative sense, its evolution was not found to differ considerably.

One may, therefore, reasonably compare the conditions in which the RWI arises in the HGB setting to the instability arising here for the symmetric-step profile. In the analysis presented in LFLC-2000, it was shown that for the HGB profile a minimum amplitude in the pressure bump was required for instability to occur. It was indicated in Fig. 9. of that study that the minimum variation required in the associated surface mass density for instability to occur, on a radial scale similar to the thickness of the disk, must be between approximately 10% to 20% (LFLC-2000). According to this study, for any given value of $0 < Q_0 < 1$, instability occurs for $0 < \Delta < \Delta_{\rm cr}$. This means that for a given peak value of the midplane enthalpy there is a maximum width size beyond which instability ceases. In this sense, the results here imply that there is no minimum required amplitude of the midplane enthalpy peak (and, consequently, the corresponding associated surface density peak) for instability to occur.

This does not necessarily mean that these results disagree with each other. Indeed in Fig. 3, it can be seen that for fixed values of Δ, there is a value of Q_0 smaller than some critical value for the system to be unstable. For example, for $\Delta = 0.7$, instability occurs for $Q_0 < 0.5$. According to Fig. 2, this means that for these parameter values the minimum midplane enthalpy peak variation over the mean must be at least 25% for instability to occur.

This still leaves open the question about the origin of the initial equilibrium. In the general scenario proposed in LFLC-2000, matter is accumulated in a piecemeal way, either by means of the coupling to large-scale magnetic field processes or due to

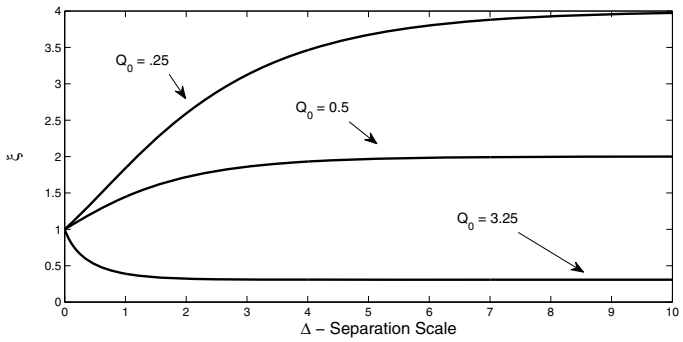

Fig. 2. Plot of ξ, the ratio of the minimum or maximum of the mean enthalpy to its value as $x \to \pm\infty$ (symmetric step profile only). Three values of Q_0 are shown: $Q_0 = 0.25, 0.5$ (depression) and $Q_0 = 3.25$ (peak).

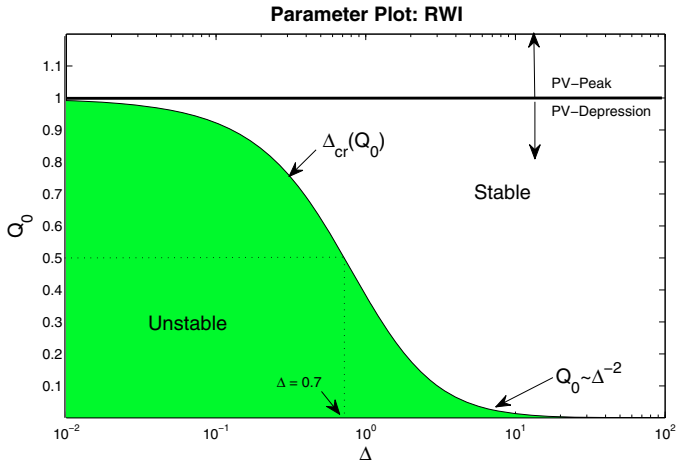

Fig. 3. Stability boundaries for the double defect problem in the $\Delta - Q_0$ plane. Unstable region depicted by shaded zone. Instability occurs for all values of enthalpy bumps (i.e., PV-depressions: $0 < Q_0 < 1$). No instability expected for enthalpy depressions. The boundary $\Delta = \Delta_{\rm cr}(Q_0)$ separates stable and unstable regions. Critical values of Q_0 corresponding to instability goes like Δ^{-2} for $\Delta \gg 1$.

small-scale turbulence (possibility MHD driven). These possibilities are not disputed here. Instead attention should be paid to the way in which matter is accumulated. Reference to Fig. 3 best illustrates this point. The way that matter accumulates depends upn the path within the Q_0-Δ plane along which the accumulation process takes place. For example, if the process involves an increase in Δ (the region size) for fixed values of $0 < Q_0 < 1$, then instability will occur before any sizeable enthalpy peak is reached because any such path (starting from $\Delta = 0$) is unstable to the RWI. On the other hand, if the initial equilibrium Q_0 is constructed on a path of constant Δ, then the system may be brought into the unstable regime with a finite large amplitude of the enthalpy peak variation. Thus, the way in which the equilibrium is constructed is crucial to assessing how and on what scale the instability will operate. This point deserves further attention in the future.

4. The single step profile in the mean PV considered in this analysis shows no instability. In contrast, the single jump profiles studied in LFLC-2000 do show the emergence of instability. The reason for this difference is not entirely clear. One possibility is that the single step profile considered here may not be a faithful analog of the single jump profile studied in LFLC-2000. Indeed, in the generalized picture of edgewave dynamics of Baines & Mitsudera (1994), one needs a minimum of two edgewaves for instability to happen. The single-defect model of this study can only support a single edgewave and, therefore, no instability is possible. A corresponding analog representation of the single jump profile considered in LFLC-2000 probably needs to support at least two edgewaves in order to see the instability expressed. This is, however, conjecture at this stage and more analysis is needed.

5. Instability can be best rationalized in terms of the interaction of the two individual edgewaves propagating along each defect of the symmetric step profile. This picture is consistent with the Hayashi-Young criterion for wave instability (Hayashi & Young 1987), which can be summarized as follows: instability of two waves separated by an evanescent layer occurs when the two waves (i) propagate opposite to each other; (ii) have almost the same Doppler-shifted frequency; and (iii) can interact with one another. Interaction in this case means that the edgewave at one defect contributes to the perturbation velocity profile at the other defect.

All of these conditions for wave instability are satisfied in the problem encountered here. In particular, one can view the Rossby-edgewaves propagating along each defect as though they were disturbances of *isolated* defects. Thus, with respect to the wavespeed calculation worked out for single isolated steps in PV (Sect. 3.1), one can write down the wavespeeds associated with each defect as

$$c_- = \frac{3}{2}\Delta - \frac{5}{2}\Theta_0 = \frac{3}{2}\Delta - \frac{5}{2}\frac{1-Q_0}{Q_0}\cdot\frac{\sqrt{Q_0}}{1+\sqrt{Q_0}},$$

for the wave at $x = -\Delta$ and

$$c_+ = -\frac{3}{2}\Delta + \frac{5}{2}\Theta_0 = -\frac{3}{2}\Delta + \frac{5}{2}\frac{1-Q_0}{Q_0}\cdot\frac{\sqrt{Q_0}}{1+\sqrt{Q_0}},$$

at $x = \Delta$. The wavespeeds $c_\pm$ and the values of c appropriate for the double-defect problem are plotted in Fig. 4[3]. It can be seen in Fig. 4b that instability occurs when the possibility exists for the two isolated waves to have nearly the same (and opposite) wavespeeds. In the rest frame $x = 0$, this occurs when each of the wavespeeds are nearly equal to zero. In Fig. 4a, where instability does not occur, the wavespeeds are not nearly equal enough (they are not close to zero), hence instability cannot occur.

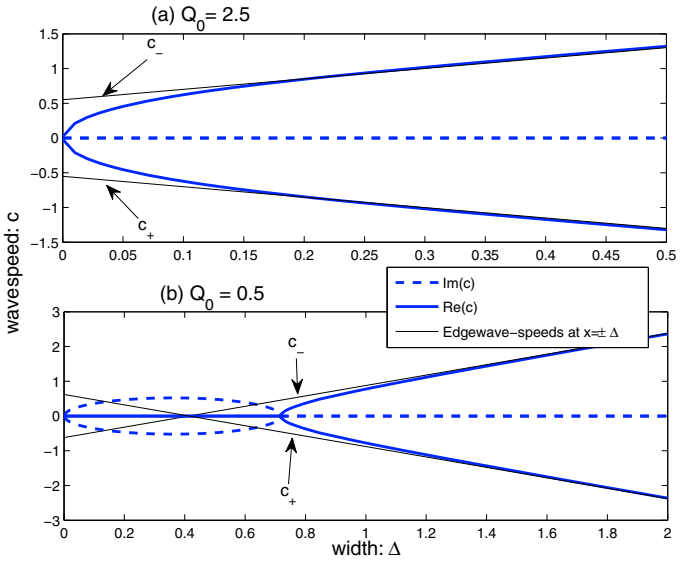

Fig. 4. wavespeeds as a function of Δ for symmetric step profile: **a)** $Q_0 = 2.5$, **b)** $Q_0 = 0.5$. Also shown are the speeds $c_\pm$ (discussed in the text, Sect. 4) corresponding to the edgewaves that would propagate along each defect *as if each defect were treated in isolation*. Instability occurs in **b)** only when these two wavespeeds are nearly equal, which is consistent with the Hayashi-Young criterion for wave instability.

In this particular double-defect setup it follows that one can roughly predict the onset of instability to be when the isolated wavespeeds are nearly zero in the reference frame of an observer at $x = 0$. Using the formula for $c_\pm$ given above, $c_\pm \approx 0$ happens very nearly when

$$\Delta \approx \frac{5}{3}\frac{1-Q_0}{Q_0}\cdot\frac{\sqrt{Q_0}}{1+\sqrt{Q_0}}.$$

Clearly this can never happen when $Q_0 > 1$ as Δ must be positive. Furthermore, when $Q_0 \ll 1$ this rough criterion means that the critical value of the separation scale is approximately

$$\Delta_{\rm cr} \sim Q_0^{-1/2},$$

which is the same trend observed in Fig. 3.

The importance of this perspective is that one may approximately assess whether or not a more complicated looking PV-profile can become unstable to the RWI instability by appealing to this conceptually simple mechanistic view. For example, if a more sophisticated PV-profile were treated as if it were a series of PV-steps, then an approximate prediction for the onset of instability would only require calculating edgewave speeds along each defect taken as though each were in isolation. Onset conditions would be predicted for values of the parameters in which any two of these wavespeeds are nearly equal.

6. The asymptotic limit that the DSW-theory exploits is one in which the azimuthal length scales are much longer than the radial ones. In this limit there is no information as to how wavespeeds depend upon the horizontal wavenumber α. In the theory developed here the wavespeed c is independent of α. However, it is known that in the vertically integrated configurations investigated in the original RWI studies there is a clear dependence of c with α.

[3] The single wavespeed formula quoted above for c_- is written in terms of the formula given in Eq. (17) augmented by the Doppler-shift consistent with the the local Keplerian speed at $x = -\Delta$. The isolated edge wavespeed c_+ is correspondingly written taking into consideration the symmetry of the mean PV-profile as viewed at $x = \Delta$, which is the opposite of that at $x = -\Delta$.

On more concrete terms, in the numerical solution shown in LFLC-2000 there is obviously a fastest growing azimuthal wavenumber of the instability, which leads to the final steady pattern state reached by the system. In contrast, in the approximate study done here for the symmetric-step profile, once stability is breached all wavenumbers become unstable and there is no high-wavenumber cut off. The growth rates, $\sigma = \alpha \mathrm{Im}(c)$, obviously increase without bound in proportion to $\alpha -$ signaling the breakdown of the theory.

To correct this issue, the DSW-theory would have to be appropriately extended by allowing for vertical structure in the horizontal velocities (i.e., inclusion of the dependence $\sim z^2$) and some deviations from the linear dependenc of the vertical velocity with the z coordinate (i.e., an additional $\sim z^3$ dependency). The resulting next order correction to the wavespeed in the extended DSW-theory will show that the general dispersion relationship takes the form

$$c^2 = \mathcal{E} + \mathcal{E}^{(2)}\alpha^2,$$

where $\mathcal{E}^{(2)}$ is a function of the parameters Q_0 and Δ. Preliminary calculations show that $\mathcal{E}^{(2)}$ is greater than zero, which means there is a high-wavenumber cutoff beyond which there would be no instability in the extended theory. The DSW-theory may be extended to higher orders in ϵ by asymptotically developing corrections for c near values of $\mathcal{E} \approx 0$, which occur for values of Δ near $\Delta_{\rm cr}$. Further investigation is needed in this regard.

7. Three-dimensional numerical simulations of the RWI were announced during the preparation of this manuscript. Meheut et al. (2010) report on three-dimensional simulations of a constant entropy disk with midplane symmetric perturbations with the main goal of following the evolution of a Gaussian bump profile in the initial pressure field. Notable features of the results show that there is a significant amount of three-dimensional structure in the horizontal velocities as well as deviations from a linear z dependence of the vertical velocities. The resultant structures show interesting and complex three-dimensional structure in the streamlines of the flow. In contrast, in the asymptotic three-dimensional theory used here the horizontal velocities have no vertical variation and the vertical velocity is linear in z. Thus, the asymptotic strategy used here is far from matching the overall structure contained in the results of these particular simulations. The DSW-theory (or an analogous approach) may be extended to capture the quality of the dynamics contained in these numerical simulations much in line with the previous comments made in this regard. Moreover, it is important to understand how the three-dimensional structure emerges in these simulations, i.e., whether it arises from other secondary barotropic processes or if they are dynamics that are tied to the primary quasi-two dimensional dynamics driven by the primary instability. Rationalization of the three-dimensional dynamics in terms of the Rossby edgewave perspective utilized in this work could be a natural first step to this end.

Acknowledgements. The author thanks Yiannis Tsapras, Oliver Gressel, Joe Barranco, and James Cho for discussions relating to this work. The author also thanks the anonymous referee for pointing out the analogy between the diocotron effect and the RWI. The author is indebted to the Kavli Institute of Theoretical Physics and the program Exoplanets Rising: Astronomy and Planetary Science at the Crossroads, where portions of this work were performed.

Appendix A: Double-defect normal-mode calculation

Following the procedure performed for the single defect, the equation $Q' = 0$ is solved separately in the three zones subject to the condition that $\hat{\Xi} \to 0$ as $x \to \pm\infty$. For $x < -\Delta$ and $x > \Delta$, the equation to be solved is

$$\partial_x^2 \hat{\Xi} - \hat{\Xi} = 0, \tag{A.1}$$

while for $-\Delta < x < \Delta$, it is

$$\partial_x^2 \hat{\Xi} - Q_0 \hat{\Xi} = 0. \tag{A.2}$$

The solution for $\hat{\Xi}$ in each of the three zones is

$$\bar{\Xi} = \begin{cases} A_- \mathrm{e}^{x+\Delta} + 1, & x < -\Delta, \\ \frac{1}{2}(A_+ + A_-)\frac{\cosh\sqrt{Q_0}x}{\cosh\sqrt{Q_0}\Delta}, & \\ \quad + \frac{1}{2}(A_+ - A_-)\frac{\sinh\sqrt{Q_0}x}{\sinh\sqrt{Q_0}\Delta}, & -\Delta < x < \Delta, \\ A_+ \mathrm{e}^{-x+\Delta} + 1, & x > \Delta. \end{cases} \tag{A.3}$$

The solution as presented satisfies the continuity of $\hat{\Xi}$ at the boundaries $x = \pm\Delta$. The remaining conditions are the continuity of the normal velocities at the location of the defects, which amounts to simultaneously satisfying

$$\left[\frac{(\bar{v}(\Delta) - 3\Delta/2 - c)\partial_x\hat{\Xi} + 2\hat{\Xi}}{1 + \partial_x^2\bar{\Xi}}\right]_{x\to\Delta^-}^{x\to\Delta^+} = 0, \tag{A.4}$$

and

$$\left[\frac{(\bar{v}(-\Delta) + 3\Delta/2 - c)\partial_x\hat{\Xi} + 2\hat{\Xi}}{1 + \partial_x^2\bar{\Xi}}\right]_{x\to-\Delta^-}^{x\to-\Delta^+} = 0. \tag{A.5}$$

These two equations result in the matrix equation

$$\mathbf{MA} = \mathbf{0},$$

where $\mathbf{M}$ is a 2×2 matrix and $\mathbf{A} = (A_+, A_-)^{\mathsf{T}}$. Nontrivial satisfaction of this matrix equation requires enforcing $\det\mathbf{M} = 0$. This results in the wavespeed relationship found in Eq. (23).

References

Baines, P. G., & Mitsudera, H. 1994, J. Fluid Mech., 276, 327
Dubrulle, B., Marie, L. , Normand, Ch., et al. 2004, A&A, 429, 1
Friedman, B. 1956, Principles and Techniques of Applied Mathematics (New York: Wiley)
Godon, P., & Livio, M. 1999, ApJ, 523, 350
Goldreich, P., & Lynden-Bell, D. 1965, MNRAS, 130, 125
Goldreich, P., Goodman, J., & Narayan, R. 1986, MNRAS, 221, 339
Hayashi, Y.-Y., & Young, W. R. 1987, J. Fluid Mech., 184, 477
Heifetz, E., Bishop, C. H., & Alpert 1999, Q. J. R. Meteorol. Soc., 125, 2835
Lovelace, R. V. E., & Hohlfeld, R. G. 1978, ApJ, 221, 51
Hoskins, B. J., McIntyre, M. E., & Robertson, A. W. 1985, Q. J. R. Meteorol. Soc., 111, 877
Knauer, W. 1966, J. App. Phys., 37, 602
Li, H., Finn, J. M., Lovelace, R. V. E., & Colgate, S. A. 2000, LFLC-2000, ApJ, 533, 1023
Li, H., Colgate, S. A., Wendroff, B., & Liska R. 2001, ApJ, 551, 874
Lovelace, R. V. E., Li, H., Colgate, S. A., & Nelson, A. F. 1999, ApJ, 513, 805
Meheut, H., Casse, F., Varniere, P., & Tagger, M. 2010, A&A, 516, A31
Papaloizou, J. C. B., & Pringle, J. E. 1984, MNRAS, 208, 721
Pedlosky, J. 1987, Geophysical Fluid Dynamics, 2nd edn. (New York: Springer-Verlag)
Lord Rayleigh 1880, Proc. Royal Math. Soc., 9, 57
Salby, M. L. 1989, Tellus, 41A, 48
Umurhan, O. M. 2006, MNRAS, 365, 85
Umurhan, O. M. 2008, A&A, 489, 953
Yavneh I., McWilliams J. C., & Molemaker M. J. 2001 J. Fluid Mech., 448, 1